



Effect of Free Stream Turbulence on Flow Past a Circular Cylinder at Low Reynolds Numbers

Vinoth Kumar¹ · Mrityunjay Singh² · Murugan Thangadurai³  · P. K. Chatterjee³

Received: 26 June 2014 / Accepted: 14 November 2017 / Published online: 9 January 2018
© The Institution of Engineers (India) 2017

Abstract Circular cylinders experiencing different upstream flow conditions have been studied for low Reynolds numbers using hot-wire anemometry and smoke flow visualizations. The upstream condition of the cylinder in the test section is varied using a wire mesh placed at the entrance of the test section. The Reynolds number is varied by varying the diameter of the cylinder and the mean velocity in the test section. Smooth cylinders of diameter varying from 1.25 to 25 mm are used in the present study. A multi-channel hot-wire anemometry is used for measuring the fluctuating velocities in the test section and the wake behind the cylinder. The sectional views of the wake behind the cylinder are obtained using a 4 MP CCD camera, 200 mJ pulsed laser and a fog generator. The flow quality in the test section is examined using higher order turbulence statistics. The effect of free stream turbulence levels and their frequencies on wake structures and the shedding frequencies of circular cylinders are studied in detail. It has been observed that the alteration in wake structure and the shedding frequency depend strongly on the frequencies and the amplitudes of upstream disturbances besides the diameter of the circular cylinder.

Keywords Wind tunnel · Circular cylinder · Hot-wire anemometry · Flow visualization · Free-stream turbulence · Higher order moments

Notations

Re	Reynolds number
D	Diameter of the cylinder
u	Mean velocity along x direction
BL	Boundary layer
x	Distance between the screen and the cylinder
y	Lateral direction from the centre of the tunnel
z	Height of the probe from the bottom of the test section

Subscripts

rms	Root mean square value of the fluctuation
mean	Time-averaged quantity of the fluctuating velocity
cr	Critical condition at which transition takes place
w	Wake width of the circular cylinder

Introduction

Circular cylinder is a most common and simplest form of the bluff body that exists in nature and several man-made structures. Flow past a circular cylinder has immense applications in engineering and applied science. For all ranges of Reynolds numbers (Re), starting from the blood flow in veins (Re ~ 100) to flow past an airplane (Re ~ 10⁶), knowledge in the circular cylinder under cross-flow is extremely important. Further, the calculation of wind loading on civil structures (Chimney stacks, Bridge piers, cables and cooling towers), hydrodynamic loading on marine structures (cables and oil pipelines in the deep ocean), Heat transfer characteristics of electrodes, nuclear fuel rods, heat exchanger tubes and electronic components in chemical, nuclear, thermal and electrical engineering, the insightful understanding in flow past the circular cylinder is vital.

It is known from last century that the alternate shedding of vortices (Karman vortex street) in the near wake of the

✉ Murugan Thangadurai
murugan.thangadurai@gmail.com

¹ Department of Aeronautical Engineering, Dhanalakshmi Srinivasan College of Engineering and Technology, Chennai 603104, Tamil Nadu, India

² Asansol Engineering College, Asansol 713305, West Bengal, India

³ CSIR-Central Mechanical Engineering Research Institute (CSIR-CMERI), Durgapur 713209, West Bengal, India

cylinder for $Re \geq 40$ leads to large fluctuating pressure forces in the transverse direction. This may cause structural vibration due to cyclic change in the direction of pressure force and production of aerodynamic noise due to velocity fluctuations in the wake. In some exceptional cases, resonance may occur which could trigger the failure of structures (Tacoma Narrows Bridge collapse [1]). The flow structures behind the circular cylinder are complex due to the interaction of three shear layers: the boundary layer (BL) over the cylinder surface resulting from no-slip, the separated shear layer due to adverse pressure gradient on the surface and the low-pressure wake behind the cylinder. Various flow regimes and variation of drag coefficient for flow past a circular cylinder at different Re are found in textbooks [2, 3] and many research papers [4–6] where the upstream velocity is assumed to be uniform.

The wake structure for various flow regimes starting from subcritical to supercritical Re has been well established based on the assumption that the upstream/free stream velocity is uniform and steady. However, the upstream flow may not be uniform in many practical situations. The disturbances created by moving, oscillating, and vibrating objects and their byproducts, that is, acoustic noise besides the changes caused by heat convection, make the atmosphere highly turbulent with large scales of vortical structures. The momentary stall and the oscillation in lift experienced by the aircraft wing in the clear air are due to the presence of small-scale atmospheric turbulence [7]. The amplitude of fluctuation in lift depends strongly on the scales of free stream turbulence (FST). For Re below 2×10^5 , the BL is extremely sensitive to the amplitude and the frequency contents of the FST [8].

The presence of various levels and intensities of FST in the atmosphere significantly alters the flow near the surface of the cylinder by energizing the fluid inside the BL which accelerates the transition to turbulence, enhances the mixing and entrainment, and distorted itself by the mean flow [9]. This causes a substantial shift in flow regimes by changing the angle of flow separation, pressure distribution, and the drag associated with the flow. The vorticity amplification theory [10, 11] suggested that the FST undergoes amplification due to vortex stretching as the flow approaches the stagnation zone of the cylinder. An important characteristic of this stretching mechanism is the selective amplification of turbulent energy at scales of vortices larger than a neutral scale. The turbulence energy dissipates more rapidly than the amplification due to viscous action at scales smaller than the neutral scale. The amplified vortices/eddies of scales which is close to the boundary layer thickness interact with the BL to induce an early transition from laminar to turbulent [12]. The earlier studies showed that the wake behind the circular cylinder, the vortex shedding frequency, and the drag coefficient have significantly altered with increased in FST for Re

up to 32,000 [13]. Here in the present study, the effect of FST is examined in detail in the low Reynolds numbers regimes.

Various levels of FST are generated inside the wind tunnel test section with the help of grids placed upstream of the circular cylinder [14, 15]. Conventionally, two types of grids (active and passive) are used in the wind tunnel depending on the level and intensity of turbulence. The passive grid produces a lesser turbulence intensity (TI) compared to the active grid due to the low root-mean-square (RMS) velocity development in the downstream [16]. The TI can be increased up to 20% using the active grid arrangement where randomly rotating agitator wing-lets add turbulent kinetic energy to the flow [17]. Since low Reynolds numbers are obtained in the present study by using the smaller cylinders which expected to have the smaller BL thickness, the free stream turbulence with less turbulence intensities are considered here.

Flow visualizations [18–20] were the only tool available to understand the behavior of real fluid flows before the seventeenth century. Leonardo Da Vinci (1452–1519) was the first person to take a scientific approach to visualize the flow. He had accurately correlated the formation of vortices with the separation of a shear layer from the lips of the leaflets [21]. The aerodynamic experiments were revolutionized by the inventions of Pitot static tube and the swirling arm in the eighteenth century. Most of the major discoveries of fluid phenomena such as transition (Osborne Reynolds), shock wave (Ernst Mach), boundary-layer (Ludwig Prandtl), Karman vortex street (Theodor von Karman) and bursting phenomena (Stephen Kline) were made through flow visualizations. Even today, the qualitative flow visualizations are used to understand the points of separation over surfaces to minimize the use of sensors in predicting the aerodynamic forces. Here, the sectional views of flow over the circular cylinder are obtained using a high energy (200 mJ/pulse) laser sheet, fog generator, and a CCD camera to identify the location of separation point over the circular cylinder and the unsteady wake. Turbulence statistics, vortex shedding and the wake width are measured using the four-channel hot-wire anemometry system. The higher order moments [22] of the fluctuating velocities are used for characterizing the flow quality at the wind tunnel [23] test section.

Experimental Setup and Instrumentation

Figure 1 shows the subsonic open circuit wind tunnel facility in CSIR-CMERI Durgapur with the smoke flow visualization and multi-channel hot-wire anemometry velocity measurement systems. It has a test section with a cross sectional area of $0.3 \times 0.3 \text{ m}^2$. The settling chamber has a square honeycomb (cell area of $0.03 \times 0.03 \text{ m}^2$) and three screens of different sizes ($0.019 \times 0.019 \text{ m}^2$, $0.013 \times 0.013 \text{ m}^2$, and



Fig. 1 Open circuit wind tunnel with experimental setup and apparatus

$0.007 \times 0.007 \text{ m}^2$) to minimize the atmospheric fluctuations inside the test section. The contraction section has an area ratio of 11 and 1 m length. It has the TI of less than 1% in the test section. The test section has a length of 1.3 m for visualizing the wake structures for long distance. The diffuser has a 4° diversion angle and a length of 1.2 m. The tunnel is operated by two counter rotating fans driven by two ac motors and variable frequency drives (VFD). The test section velocity can be varied from 0.4 to 35 m/s.

The laboratory ambient temperature is maintained using split air conditioners and the relative humidity is maintained with the help of a dehumidifier (Origin, Novita). The local temperature and pressure are measured using the analog barometer and a digital thermometer from SATO. The average velocity at the test section is measured using a four in one DP measurements micro-manometer and a Pitot static tube. A four channel hot-wire anemometry system is used for measuring the fluctuating velocities. The hot-wire probes are calibrated against the micro-manometer before being used for measuring the turbulence statistics in the wind tunnel. The FST in the test section is altered using a wire mesh with the average cell size of $5.3 \times 5.3 \text{ mm}$ and the diameter of 1.15 mm. The effect of Reynolds numbers and FST are studied by placing the circular cylinders of different diameters at different axial locations where the FST statistics are known. The data acquisition is performed using the NI PXIe-1062Q chassis (eight slots) with the NI PXIe-8133 controller. LABVIEW program is used for acquiring and analyzing the fluctuating velocity data.

Smoke flow visualization is performed using a laser sheet from 532 nm, 200 mJ/pulse and 15 Hz double pulsed Nd: YAG laser (Quantel, France) and a 4 MP power view plus CCD camera. The flow is seeded with the particles of

10μ size using an Antari fog machine (Z-1200 II). The laser and the camera are synchronized with a 250 ps resolution laser pulse synchronizer from TSI, India. The position of the camera is varied using a two axis traverse system placed at the bottom of the test section. Many experiments are performed to optimize the smoke concentration for capturing the separation point and the vortex shedding. Adjusting the smoke intensity and the position of the fog generator were highly challenging as the smoke was fed from outside the settling chamber. This method is expected to give an accurate prediction of separation point compared to the streamlined smoke layers generated through discrete points in the upstream of the cylinder.

Results and Discussion

The ambient air density in the laboratory is calculated using the pressure measured from an analog barometric and the temperature measured with a digital thermometer. The fluid viscosity is calculated using Sutherland's formula from measured temperature. Reynolds number (Re) is calculated using the calculated density and viscosity. It is varied by changing the cylinder diameters and the test section velocity. The flow can be assumed two-dimensional as the cylinders have a maximum deviation of $\pm 0.03 \text{ mm}$ from the mean diameter. Hot-wire probes are mounted on a rack and traversed across the test section to obtain the fluctuating velocity from which turbulence statistics are obtained.

TI is defined as the ratio of root mean square of velocity fluctuations to the mean velocity which shows the level of fluctuations in the wind tunnel. The probability density function (PDF) shows the skewness (deviation from the

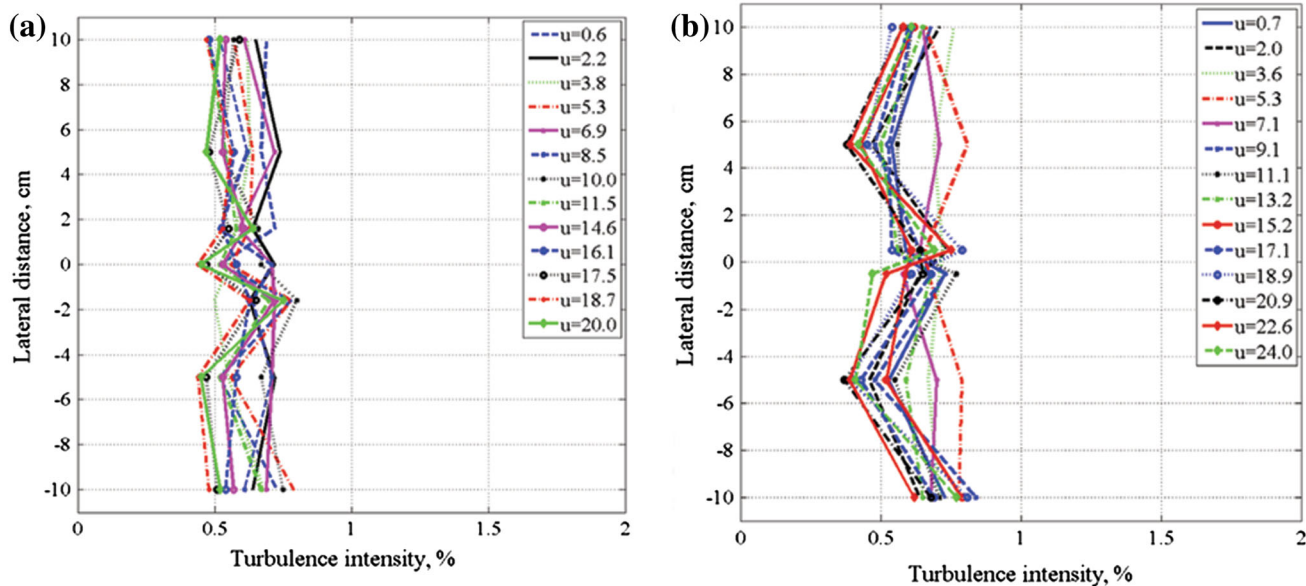


Fig. 2 Turbulence intensities at **a** $x = 120$ mm, **b** $x = 220$ mm across the test section

symmetric distribution) in the signal qualitatively. Conventionally, the skewness near the wall is linked to the bursting process in turbulence [24]. The flatness factor describes the deviation of Gaussian profile especially the flatness of the tail. If the PDF has relatively large values in its tails, then the flatness value will be larger [25]. This occurs when the time series data contain significant numbers of sharp peaks and it is related to the intermittency [26].

Here, the flow quality in the test section is examined first using the turbulence statistics obtained from the fluctuating velocities as it has a strong effect on the flow separation and vortex shedding. Next, the effect of empty tunnel disturbances on the past a circular cylinder from $Re = 31$ to $Re = 466$ is presented using flow visualizations and fast Fourier transform (FFT). The effect of increased level of FST (3%) on the cylinder wake is compared with the empty tunnel FST (0.3%) in the subsequent section. Finally, the variation in wake structure for different diameters of the circular cylinder with same Re and variation in FST is discussed.

Examination of Flow Quality in the Test Section

Each and every wind tunnel existing around the world has a certain level of free stream turbulence (FST) and it depends on the local ambient, the honeycomb, number of screens and the contraction ratio. The size and distribution of eddies/vortices present in the free stream flow have a dominant role on the deviation of various scaled model results. It is essential to have the quantitative measurement of these upstream disturbances. TI is traditionally used to describe the flow quality at the test section. However, the flow may have some shear due to non-

uniformity in the screens inside the settling chamber, rough wall and leakages in the test section even though the TI is constant in the test section for small test section wind tunnels. The shear layers induced in the flow due to leakage at the test section wall was observed using higher order moments of fluctuating signal [21]. The hot-wire probes used for measuring the fluctuating velocities are calibrated in the wind tunnel against the steady velocity measured using a Pitot static tube and micro-manometer. The calibration coefficients are obtained from curve fitting in MATLAB using the King's law.

Figure 2 shows the percentage variation of TI measured across the test section (y) at six locations and two locations in the axial direction (x) where $x = 0$ represents the starting position of the test section. The hot-wire probes are kept at 140 mm from the bottom of the test section (z). The data are acquired at 10 kHz sampling rate for 10 s at each location and it is repeated for five times with the overheat ratio (OHR) of 1.6. The turbulence intensities are measured just upstream of the cylinder locations before the cylinder being placed to study the FST effects. The average percentage variation of empty tunnel TI is around 0.3% for the velocities range considered in the present study. In order to find the existence of shear in the flow, the PDF of the fluctuating velocity signal is analyzed. Figure 3 shows the Gaussian (normal) distribution of the fluctuating velocity signal [20]. Ideally, the flatness factor of the Gaussian distribution is three and the skewness factor is zero for the uniform wind tunnel velocities. However, the presence of FST in the test section cause slight deviation in these values. A small variation in the value of skewness and flatness factors in Fig. 3 guarantees that the flow is almost uniform throughout the test section.

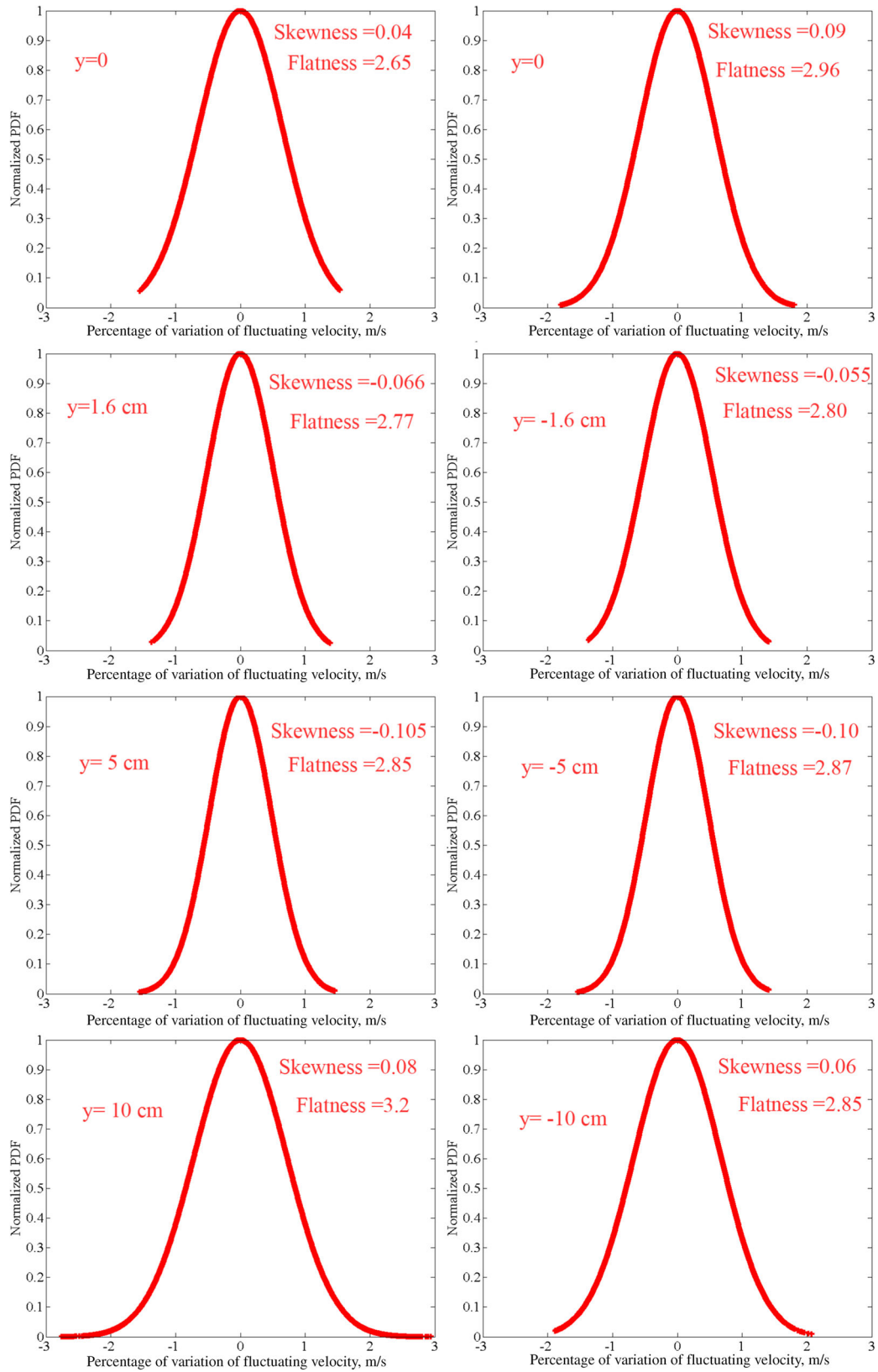


Fig. 3 Probability density function (PDF) at different lateral locations across the test section

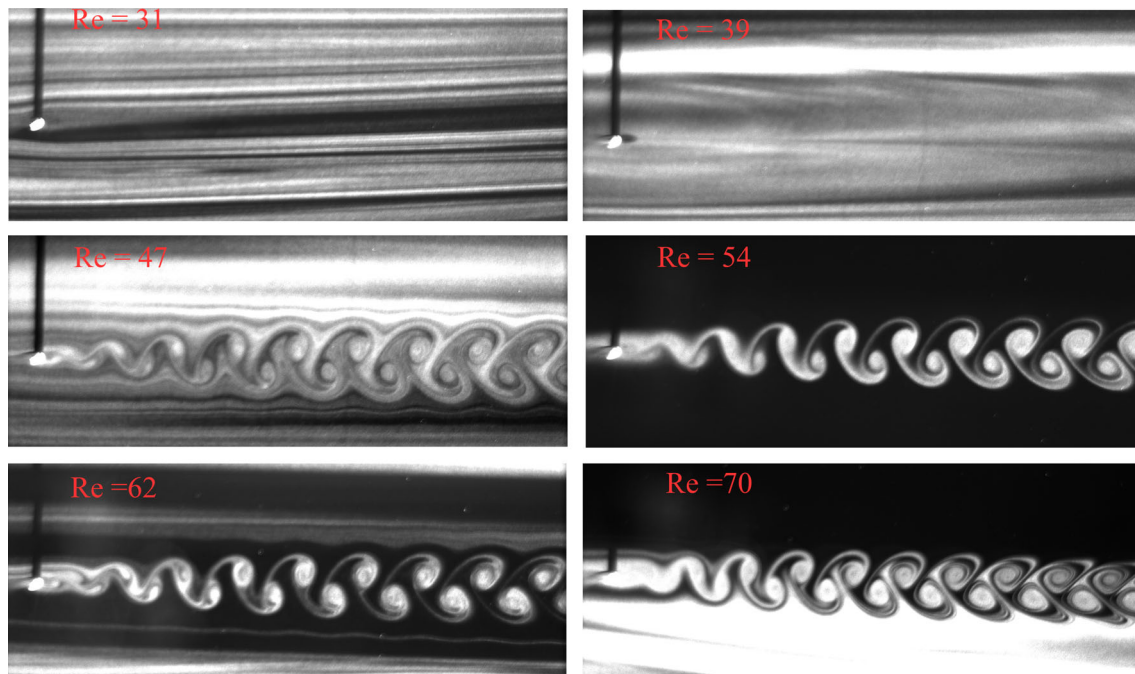


Fig. 4 Smoke flow visualization of flow past a circular cylinder for Re from 31 to 70

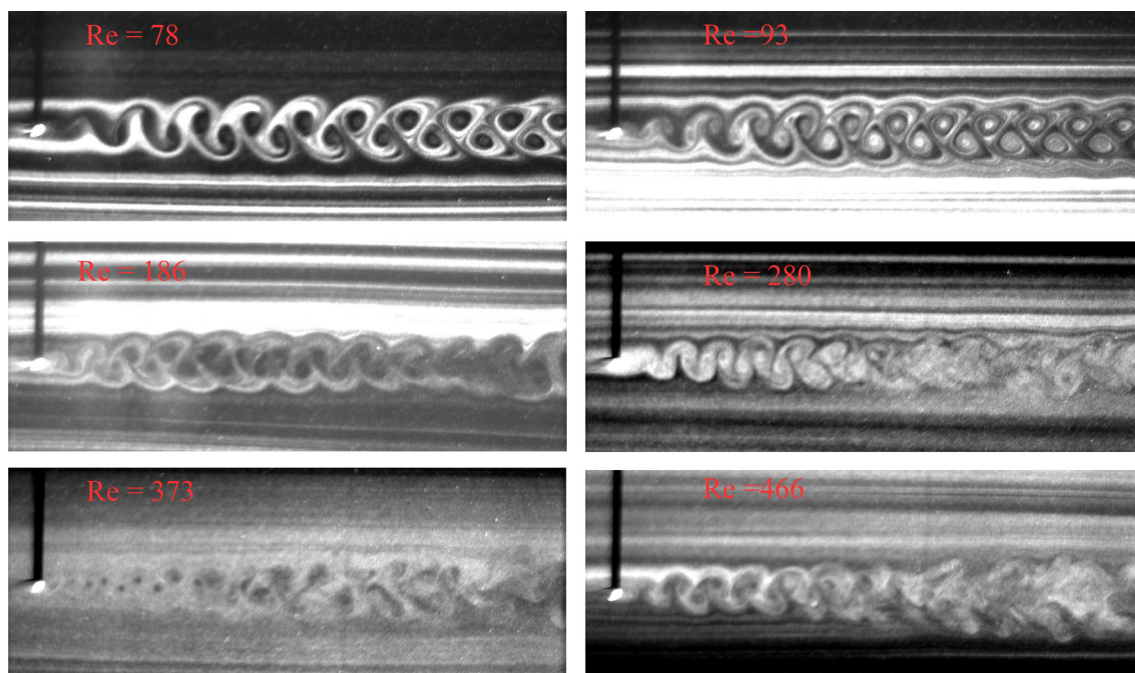


Fig. 5 Smoke flow visualization for Re from 78 to 466

Effect of Empty Tunnel FST on Transition

Figures 4 and 5 show the smoke flow visualizations of flow past circular cylinder for Re varying from 31 to 466. Here, a circular cylinder of 1.25 mm diameter is placed at the middle of the test section. The flow is seeded with water-

based particles from outside the settling chamber and it is illuminated with 2 mm thickness laser sheets. A camera placed under the test section captures the evolution of the wake. The reflection of laser light causes a small over-exposed zone at the cylinder surface. A small recirculation zone is observed behind the cylinder for Re = 31 which

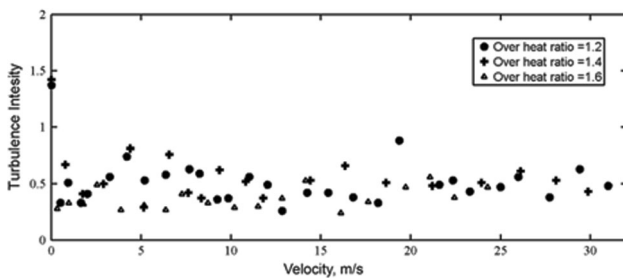


Fig. 6 Variation of TI with free stream velocity and OHR

grows as the Re increases ($Re = 39$). An alternative shedding of vortices from the cylinder is seen at $Re = 47$. Traditionally, the transition and shedding pattern behind the cylinder in a uniform flow is characterized by non-dimensional frequency or the Strouhal number [27]. However, the uniform flow without disturbances is very difficult to obtain in practical fluid flow simulations.

The free stream turbulence levels, acoustic disturbances, cylinder roughness, cylinder aspect ratio, end conditions, and blockage ratio affect the transition over the circular cylinder [4]. The critical Reynolds number (Re_{cr}) at which the onset of Karman vortex shedding (KVS) is seen depends strongly on upstream condition if the cylinder is

smooth and the aspect ratio is large with a negligible blockage ratio and acoustic disturbances. The Re_{cr} is not a universal constant and it takes a different value for different initial conditions of the flow [28]. The flow created in a highly viscous oil showed the highest Re_{cr} and the onset of KVS was observed at $Re = 65.2$ [29] where the background disturbances are dissipated quickly due to strong viscosity. Many other experimental studies in the wind tunnel have also shown a large scattering of Re_{cr} varying between 40 and 65.2 [29, 30].

Figure 6 shows the variation of TI for three overheat ratios (OHR) in the middle of the test section. The average variation of TI is around 0.4% for velocity up to 30 m/s and it becomes 0.3% for lower velocities (up to 10 m/s). Figure 7 shows the empty tunnel frequency spectra obtained using FFT for $Re = 31, 39, 44$ and 47 based on the circular cylinder diameter of 1.25 mm. Though the TI is almost similar, the frequencies which dominate the flow at different speeds are different. Hundred (100) Hz frequency dominates the flow at velocity 0.38 ($Re = 31$) and 0.47 m/s ($Re = 39$). However, four frequencies (35, 50, 100, and 355 Hz) dominate the flow at 0.53 ($Re = 43$) and 0.58 m/s ($Re = 47$) where the transition expected to occur. A simple calculation based on frequency and velocity shows that eddies of sizes 1.5, 5.3, 10,

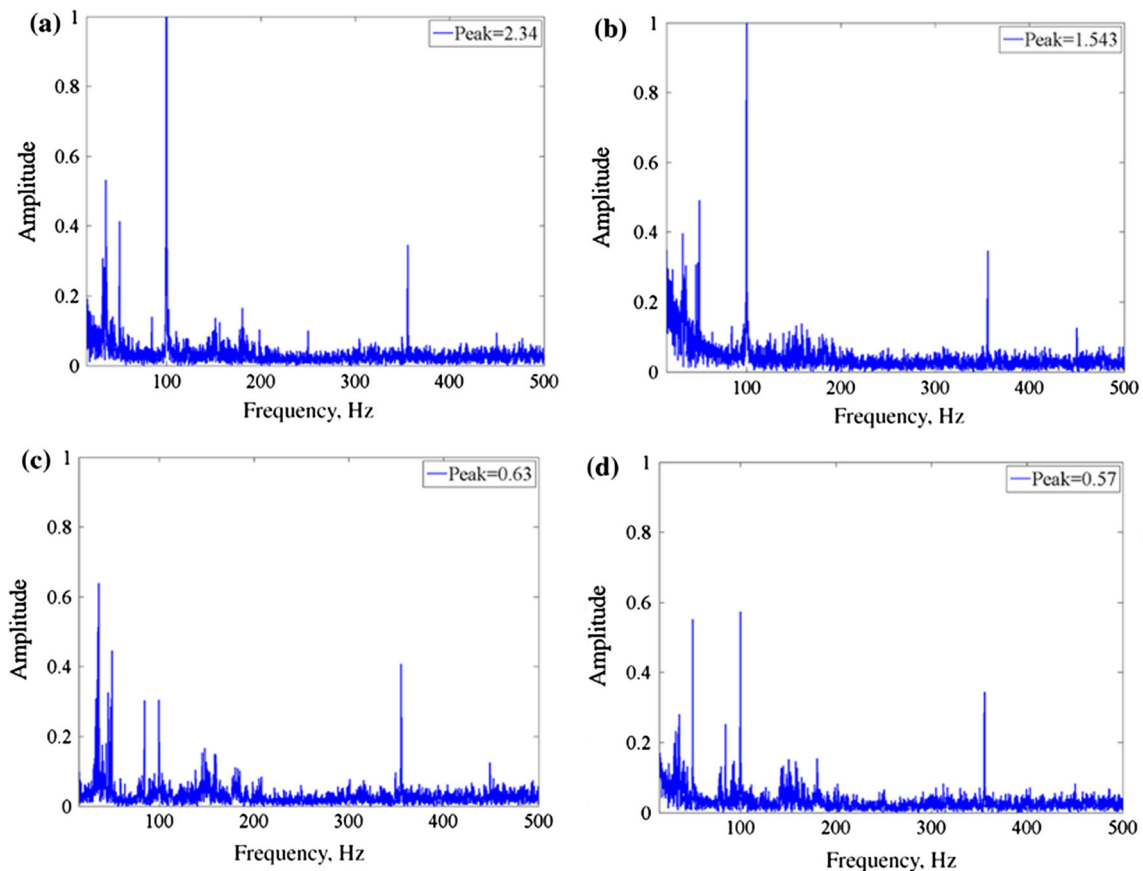


Fig. 7 Power spectra of empty tunnel data at $Re =$ **a** 31, **b** 38, **c** 44 and **d** 47

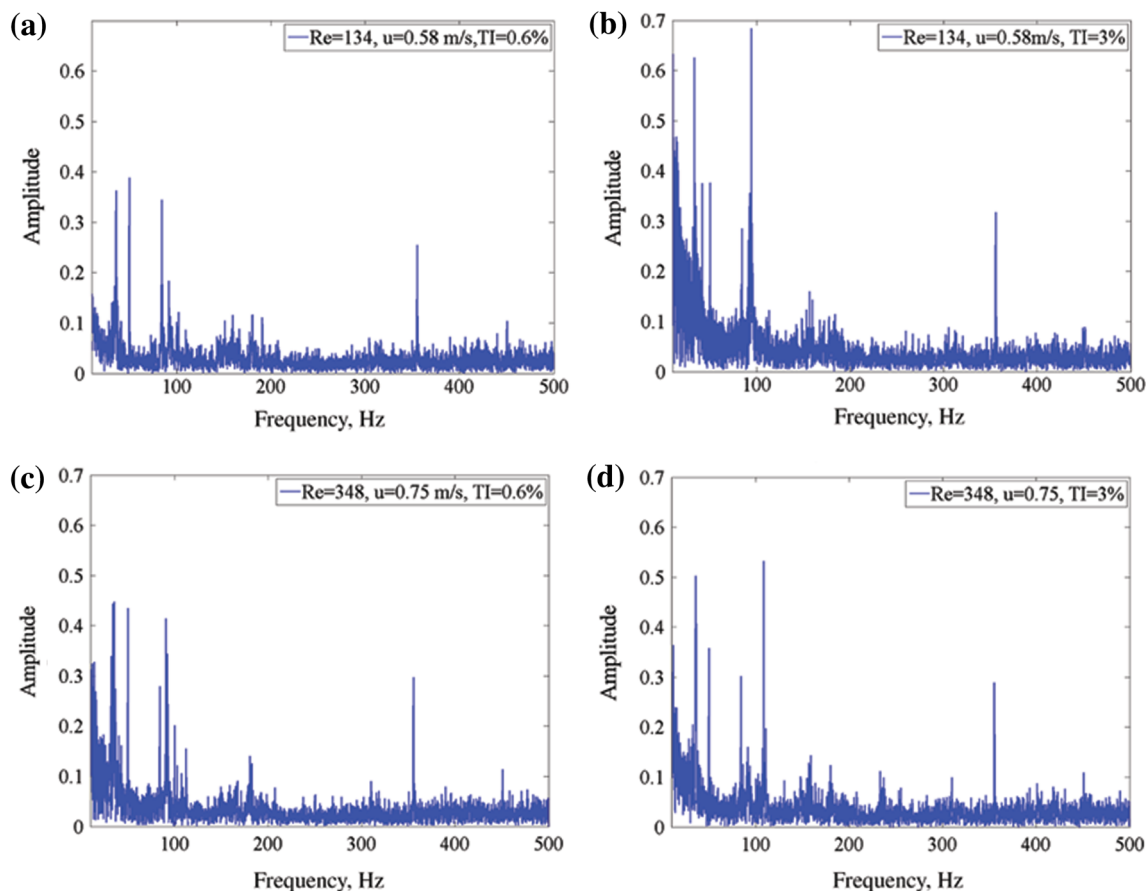


Fig. 8 FFT at an upstream location of the cylinder for $u =$ **a, b** 0.58 m/s and **c, d** 0.75 m/s with the FST of 0.6 and 3%

and 15 mm dominate the flow. Either one or few dominant frequencies may be responsible for the flow transition and vortex shedding in Fig. 4 at $Re = 47$.

The vortex shedding frequency increases with increase in Re due to lesser formation time of vortices behind the cylinder. The flow in the cylinder wake (vortex shedding region) is laminar at $Re = 47$ and 93 in Fig. 5. It was shown in the literature [4] that the transition in wake appears at Re ranging from 180 to 194. The dissipated smoke regions in the Karman vortex sheet near the cylinder at $Re = 186$ shows the fluid transition in the wake. The far downstream has already become turbulent and the clear vortex shedding pattern is no longer identified. The fine-scale three-dimensionality in the wake near the cylinder becomes increasingly active as Re increases, which causes vortices to become turbulence structures at $Re = 373$ and above.

Effect of High Level FST on Wake Structure

The effect of increased level of FST in the wake of the circular cylinder for Re up to 5441 is shown in this section. The FST level ahead of circular cylinders in the test section is

varied using a wire mesh with an average cell size of $5.3 \text{ mm} \times 5.3 \text{ mm}$ where the wire thickness is 1.15 mm. The measured TI near the wire mesh is around 8% and it reduces along the downstream direction [15]. The measured TI near the wire mesh is around 8% and it reduces along the downstream direction [15]. The reduction of TI with distance can be attributed to the breakdown of larger vortical structures and the energy transfer from large scale structures to small scale eddies. The circular cylinders are placed at 130 mm downstream of the wire mesh where the TI is 3%.

Figure 8 shows the power spectra obtained at an upstream location of the cylinder without the presence of cylinder for the above Re with two FST levels. FFT algorithm in the MATLAB is used for calculating the dominant frequencies in the signal. Here, an increase in FST from 0.3 to 3% has altered the frequencies and their amplitude in the velocity signal. The base tunnel flow ($TI = 0.3\%$) is dominated by 40, 50, 100 and 350 Hz frequencies and their amplitudes are also comparable. Increasing the TI by a wire mesh has enhanced the amplitude of 40 and 100 Hz frequencies besides amplification of few additional frequencies.

Figures 9 and 10 show the flow visualization images obtained for $Re = 134$ (3.5 mm cylinder) and $Re = 348$

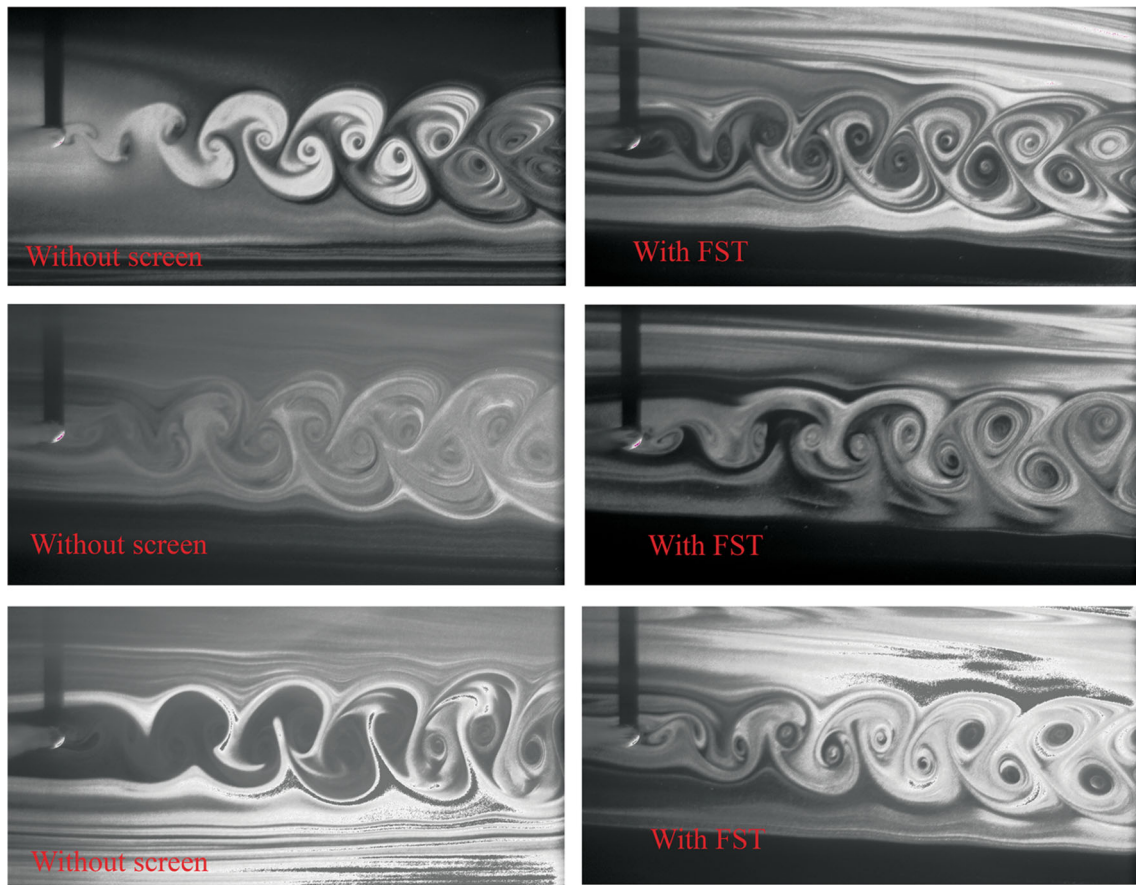


Fig. 9 Karman vortex shedding behind the circular cylinder at $Re = 134$

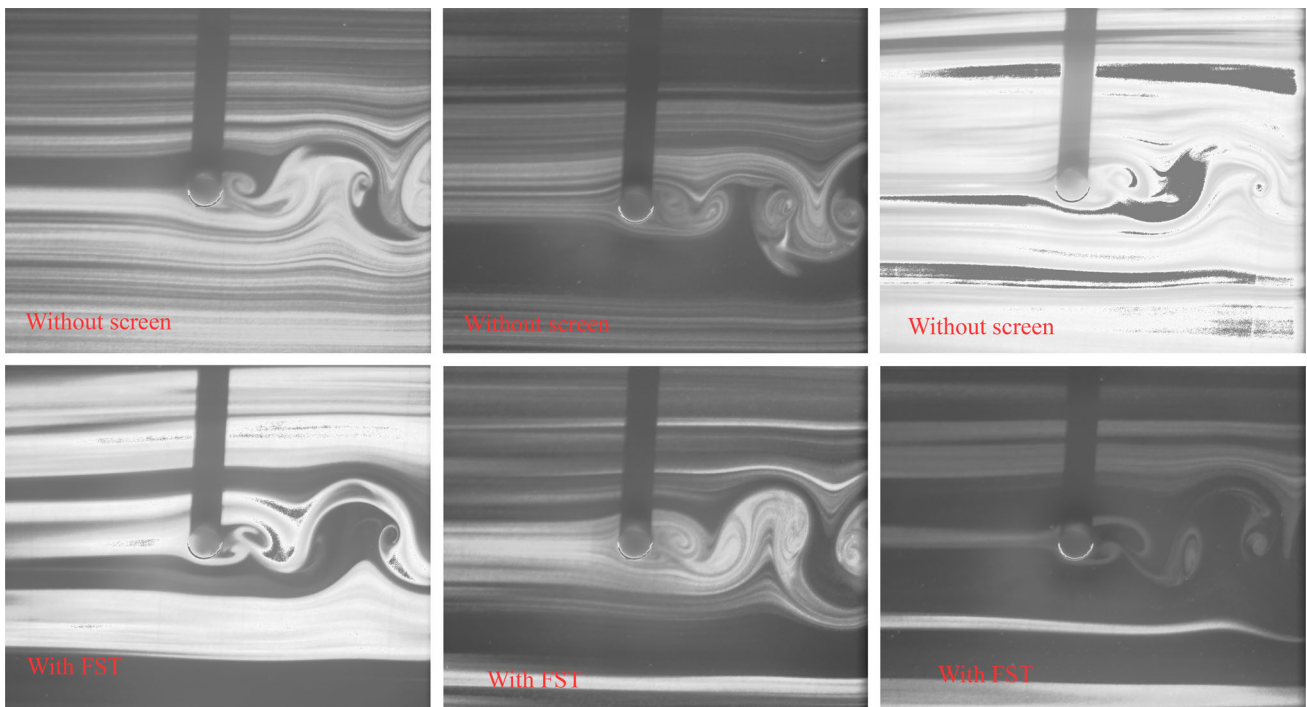


Fig. 10 Karman vortex shedding behind the circular cylinder at $Re = 348$

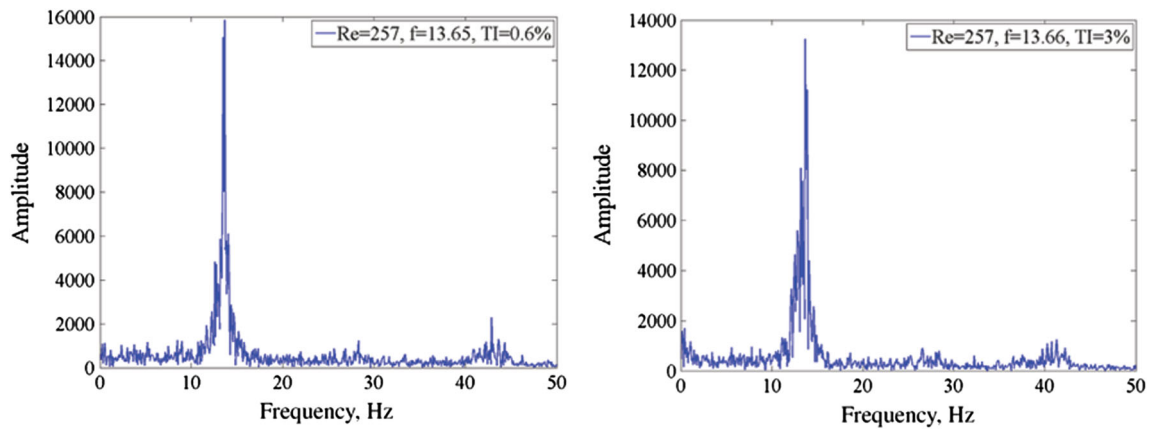


Fig. 11 Power spectra of dominant shedding frequency for $Re = 257$ with TI of 0.3 and 3%

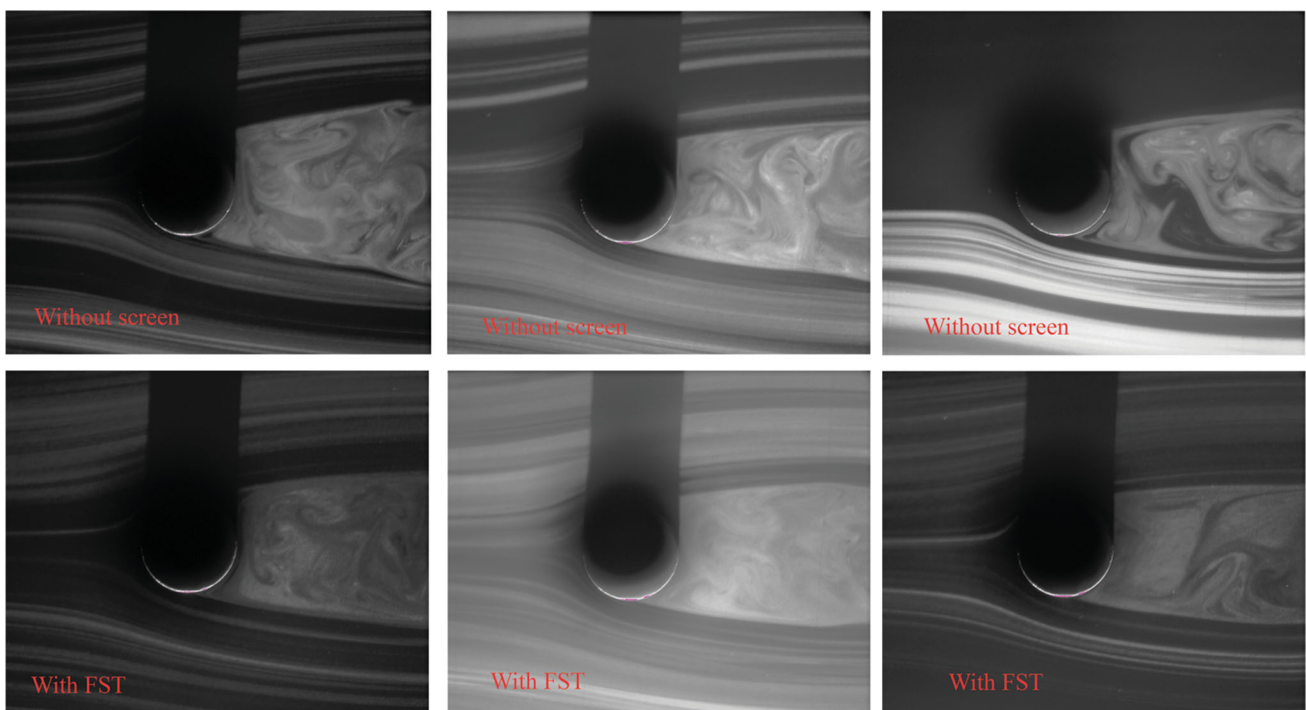


Fig. 12 Effect of change in FST on cylinder wake at $Re = 746$

(7 mm cylinder) with the TI of 0.3% (empty tunnel FST) and 3% (with grid). The corresponding velocities for these Reynolds numbers are 0.58 and 0.75 m/s. Here, though both near-field (Fig. 9) and far field (Fig. 8) wake structures look similar, the effect of an increase in FST level from 0.3 to 3% can only be seen outside the wake through the diffused smoke streak lines. Further, the separation point over the cylinder is very difficult to identify due to the smaller diameter of the cylinder.

Quantitative validation is performed by examining the frequency contents existing in the cylinder wake. Here, the dominant frequencies of vortex shedding are obtained by traversing the hot-wire probe across the wake which is

expected to give the accurate value and minimize the uncertainties. Figure 11 shows the vortex shedding frequency obtained for $Re = 257$ which is in between $Re = 134$ and 348 with the TI of 0.3 and 3% where the cylinder diameter is 7 mm. It can be seen from the figure that the shedding frequency is almost same for both FST intensities. This shows that the increased momentum transport from the FST cannot reach close to the cylinder surface to alter the transition due to high viscous forces in these Reynolds numbers.

Figures 12, 13, 14 and 15 show the wake structure behind the cylinder for higher Reynolds numbers varying from 746 to 1555 where the distinct KVS cannot be

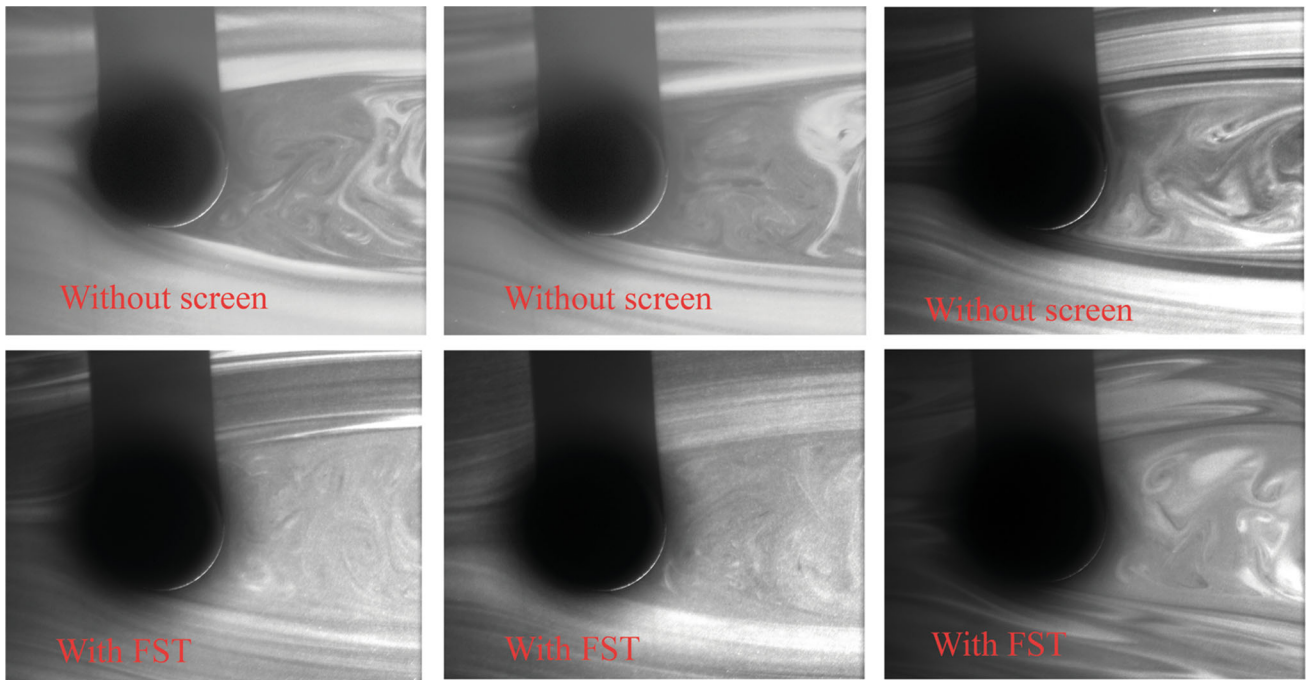


Fig. 13 Effect of change in FST on cylinder wake at $Re = 933$

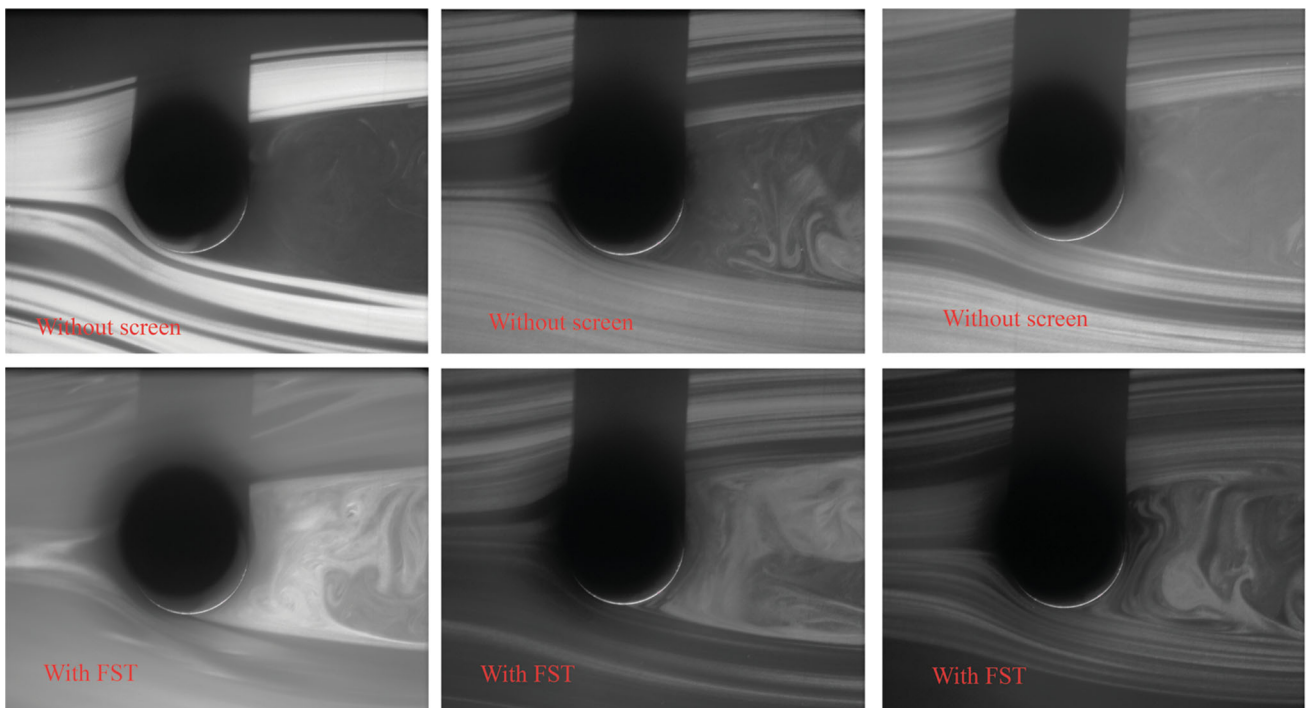


Fig. 14 Effect of change in FST on cylinder wake at $Re = 1244$

observed due to the turbulent nature of the wake at these Re . Cylinder with a diameter of 15 mm is used for $Re = 746$ ($u = 0.57$ m/s). However, a 25 mm diameter cylinder is used for $Re = 933$ ($u = 0.57$ m/s), 1244 ($u = 0.75$ m/s) and 1555 ($u = 0.95$ m/s). The frequency

contents of the base tunnel velocity signals are same to Fig. 8 as the test section velocities are low. A notable decrease in wake width is observed at different downstream locations when the FST intensity is increased from 0.3 to 3% for all these Reynolds numbers though the separation

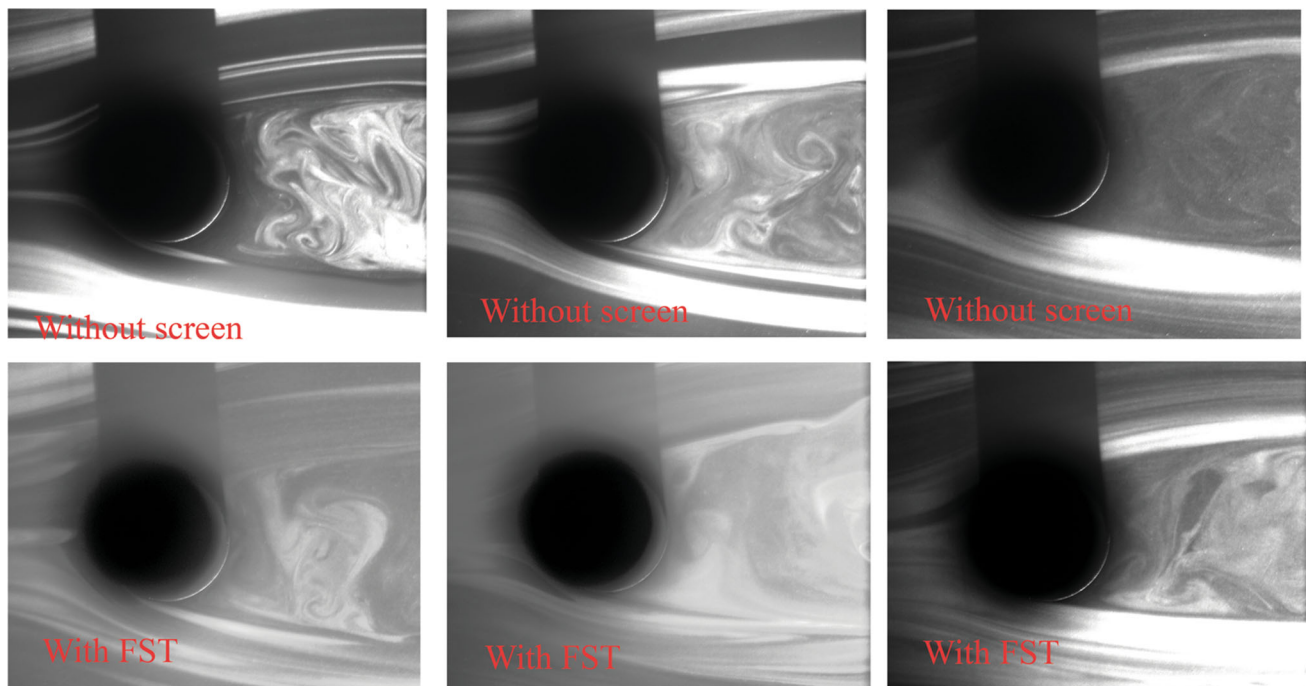


Fig. 15 Effect of change in FST on cylinder wake at $Re = 1555$

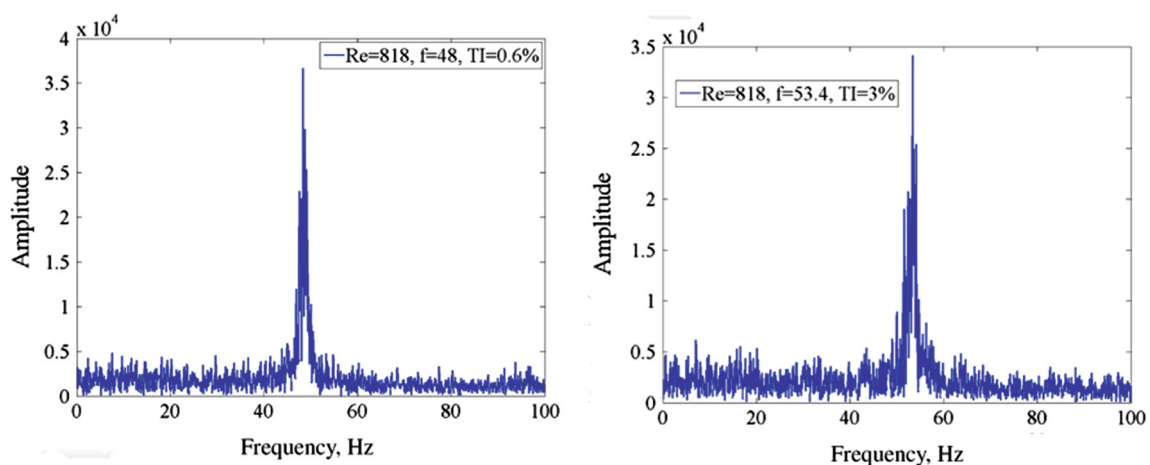


Fig. 16 Power spectra behind the cylinder wake at $Re = 818$ with the FST of 0.6 and 3%

points over the cylinder are difficult to measure quantitatively.

Figure 16 shows the shedding frequencies obtained with the FST intensities of 0.3 and 3% for $Re = 818$ (diameter of the cylinder is 7 mm) to quantify the effect of FST. A significant increase in shedding frequency is observed at this Re . This increase in frequency shows the formation of smaller KVS vortices which reflects the delay in flow separation and a decrease in wake width. Further increase in Re with 3% FST also increases the shedding frequencies which can be seen from Fig. 17. This clearly shows that the small scale eddies present in the mean flow could overcome the viscous forces in the boundary layer and

penetrate close to the wall to induce boundary layer transition at these Reynolds numbers.

Figure 18 shows the variation of non-dimensional wake width for $Re = 746$ and 1244 with two FST levels of 0.6 and 3%. Here, W denotes the width of the wake and D represents the diameter of the cylinder. The wake width is measured from a number of flow visualization images at 1 D downstream location from the cylinder rear end. A substantial increase in wake widths is noticed with increased FST though the boundary layer over the cylinder is expected to laminar (strong viscous forces) in these Reynolds numbers. The wake width for $Re = 1244$ is significantly increased compared to $Re = 746$. This

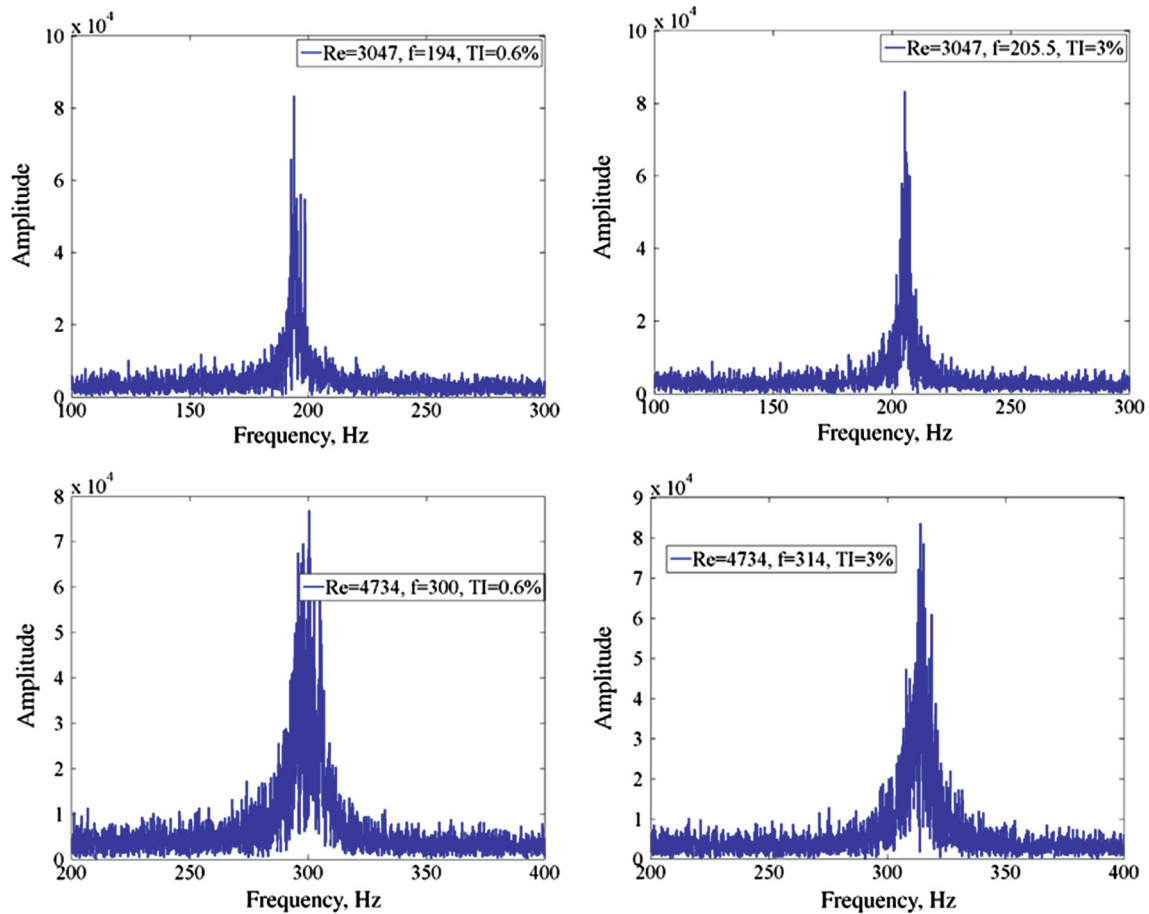


Fig. 17 Vortex shedding frequencies for $Re = 3047$ and 4734 with the FST of 0.6 and 3%

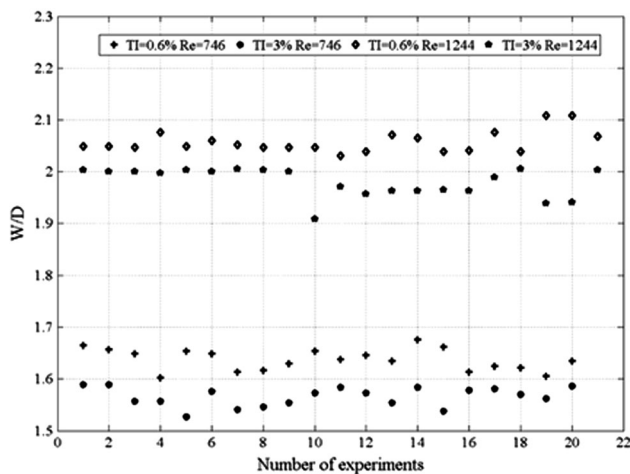


Fig. 18 Effect of FST on wake width for $Re = 746$ and 1244

indicates an early transition and delay of separation point over the cylinder surface with increased FST.

The vortex shedding pattern behind the circular cylinder for same Re is also expected to change with a change in FST besides shedding frequencies shown above. The

alteration in shedding patterns with a change in FST at low Reynolds numbers ($Re = 45$ and 53) was shown in literature [14] by varying the free stream velocity and the cylinder diameter. Here, the variation in wake profiles for higher Reynolds numbers ($Re = 933, 1555, 3110$ and 5441) with a change in FST from 0.3 to 3% is shown in Figs. 19 and 20. Two cylinder diameters of 15 and 25 mm are used and the Re is fixed by varying the free stream velocity. The wake profile is completely different for two different diameters of the cylinder, though the Re is same. This shows that the consequences of FST on different diameter cylinders (variation in boundary layer thickness) are different though Re is same.

It is also interesting to note here that the shedding frequency decreases with a decrease in free stream velocity and an increase in diameter of the cylinder. Figure 21 shows the power spectra obtained at the 25 mm diameter cylinder wake for $Re = 4432$ and $13,297$ with the FST levels of 0.6 and 3%. The shedding frequency increases with an increase in FST at these Re as well. A percentage increase of 2 and 4% in shedding frequency is noticed for $Re = 4432$ and $13,297$. However, the shedding frequency

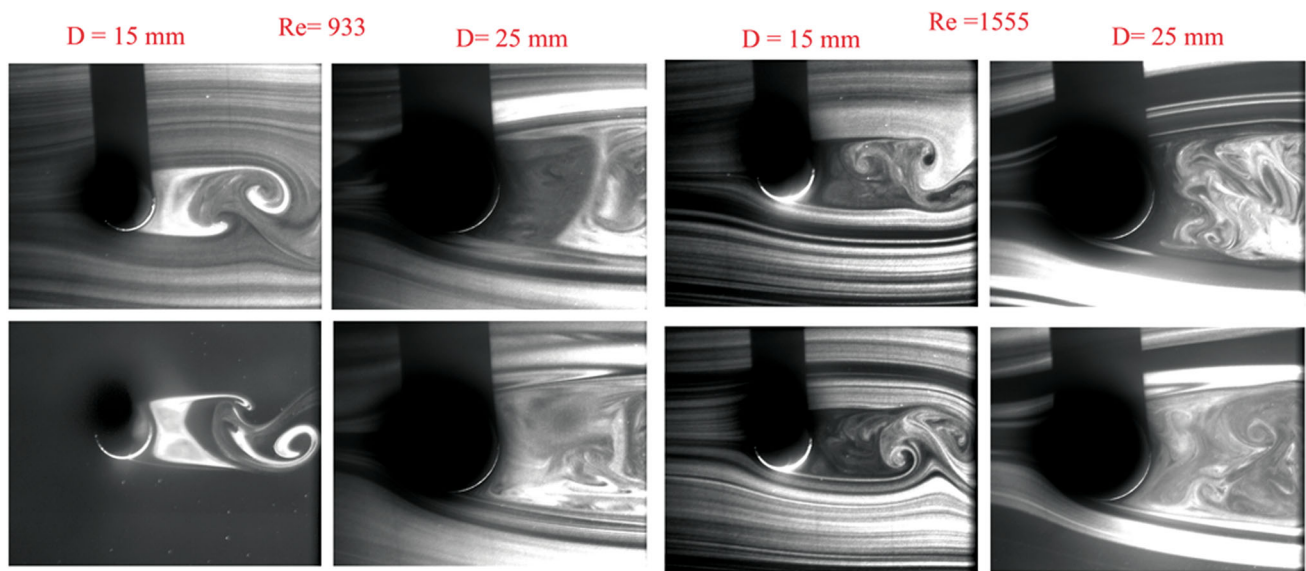


Fig. 19 Variation of wake structures with change in diameters for $Re = 933$ and 1555

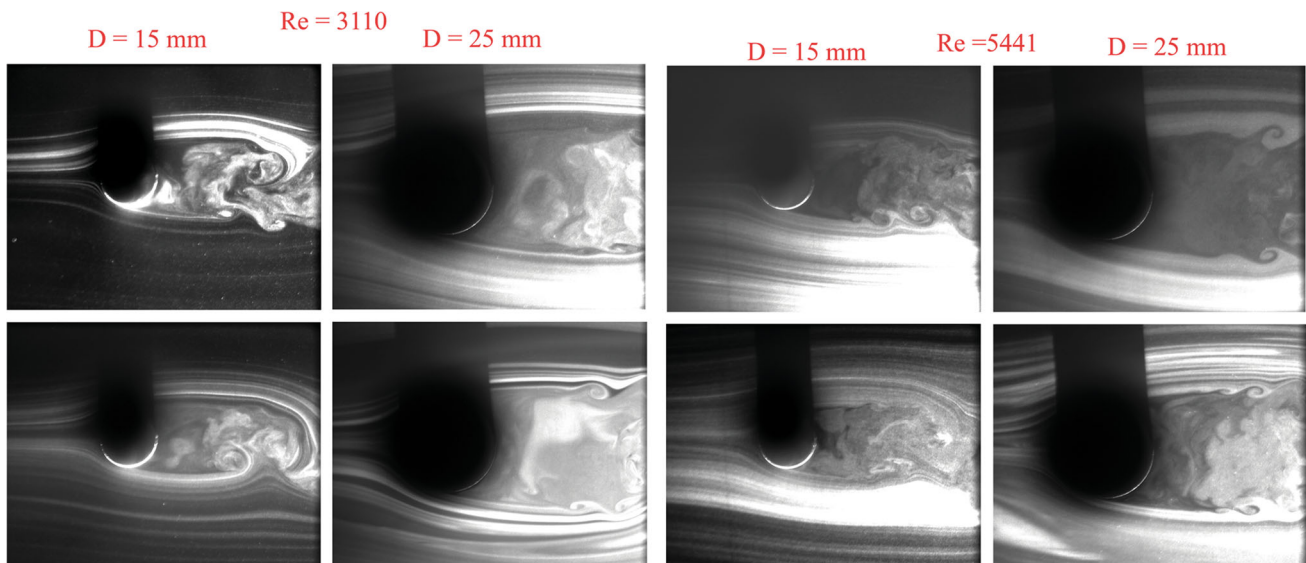


Fig. 20 Variation of wake structures with change in diameters for $Re = 3110$ and 5441

with 25 mm diameter cylinder at $Re = 4432$ with 3% FST is 23 Hz which is much lower than the shedding frequency (205.5) of 7 mm cylinder at even lesser Re (3047).

The percentage variation in shedding frequency is reduced from 4.5 (Fig. 17) to 2% (Fig. 21) by increasing the diameter of the cylinder for a similar range of Re (4734 and 4432) with 7 and 25 mm diameter cylinders. This implies that dominant frequencies existing in the free stream with 3% FST can have an influence on separation over the cylinder up to a certain diameter of the cylinder and velocity. Beyond which it may not have any effect, as these frequencies are expected to be suppressed by the strong viscous action in the boundary layer before reaching the transition point in the laminar region (80°)

for larger diameter cylinders. However, this limit of cylinder diameter is not obtained due to the smaller test section as the blockage ratio beyond 5% plays a major role in the transition.

The above flow visualizations and FFT data have clearly shown that the FST frequencies and their amplitude of certain limit can affect only up to a certain diameter of the cylinder. In most of the real-life scenarios, smaller diameter cylinders (suspension bridges, [1]) are highly affected by atmospheric turbulence rather than larger diameter cylinders (cooling tower, storage tank). The FST frequencies and their amplitudes have to be changed if the transition is desired at higher diameter cylinders. A huge spectrum of frequencies with different amplitude levels can

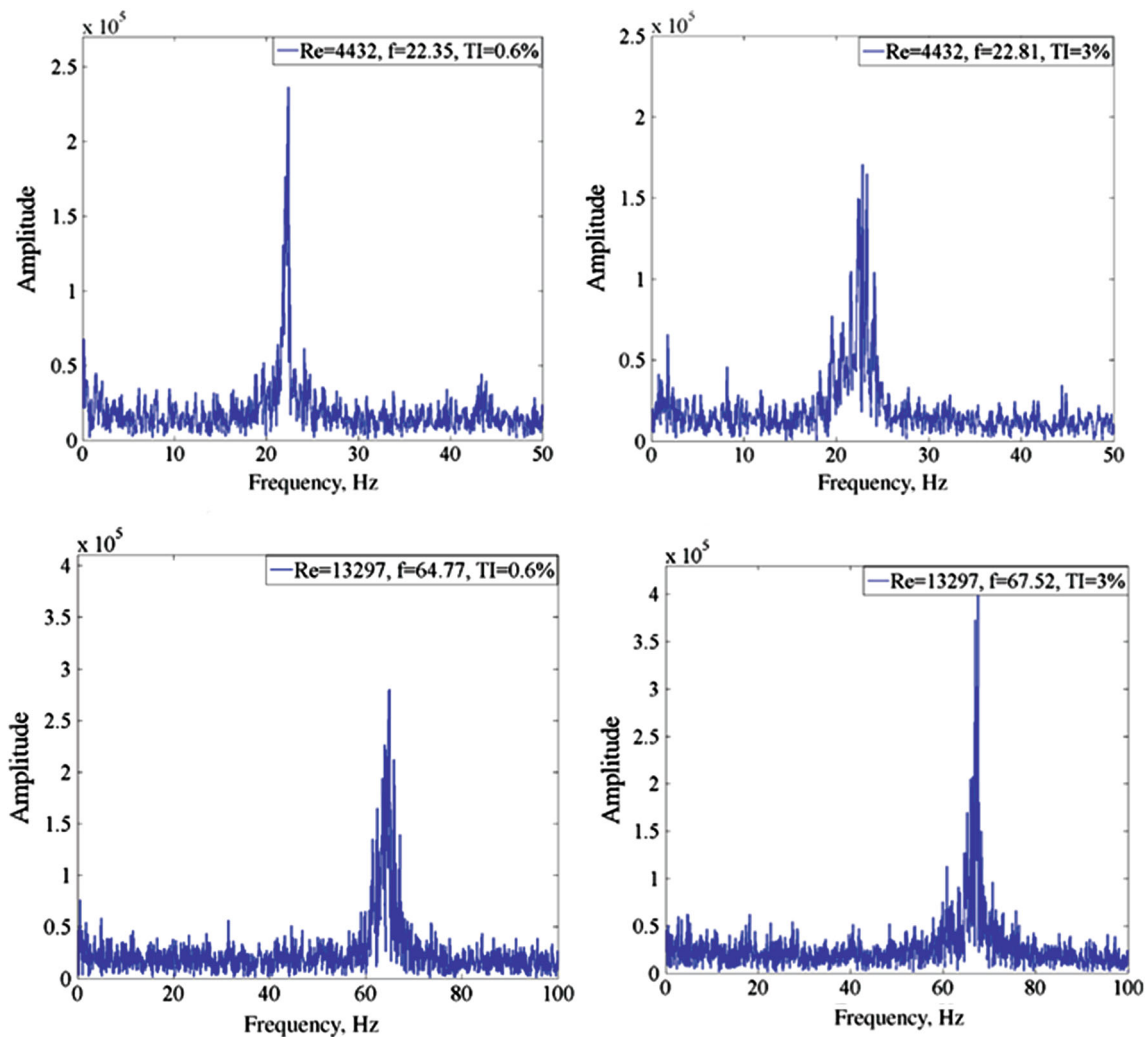


Fig. 21 Vortex shedding frequencies for $Re = 4432$ and $13,297$ with the FST of 0.6 and 3%

be generated through active grid mechanism rather than the passive grid used in the present study. A randomly rotating agitator winglets were used in the literature [17] for producing the free stream flow with 20% TI. A similar configuration will be used for controlling the frequencies and amplitudes of FST in our future studies.

Conclusion

Effects of change in free stream turbulence on the flow past a circular cylinder have been studied using hotwire anemometry and smoke flow visualization for Reynolds number varying from 31 to $15,000$. The flow quality in the test section was examined using probability density function, TI and the higher order moments of turbulent fluctuations as the free stream conditions have a strong role in the transition over the circular cylinder. It has been observed that the higher order moments have small

variations across the test section. This implied that the mean flow is uniform with a constant TI across the tunnel. The empty tunnel has a free stream turbulence (FST) with the average TI of 0.3% . The smoke flow visualizations showed that the transition in the wake and vortex shedding behind the circular cylinder is observed between $Re = 42$ and 45 for the wind tunnel in CSIR-CMERI Durgapur. Earlier experimental studies have shown a range of Re from 40 to 65.2 for vortex shedding depending on the disturbance in the test section.

The dominant frequencies ($40, 50, 100, 350$ Hz) in the free stream and their amplitude were changed (40 and 100 Hz) when a wire mesh was placed at the entrance of the test section. A maximum TI of 8% was observed close to the wire mesh and it reduces along the downstream direction due to the breakdown of larger vortical structures and the energy transfer from large scale structures to small scale eddies and the subsequent dissipation in Kolmogorov length scales. Cylinders of different diameters were placed

at the location of known TI (3%) to study the effect of FST. Both flow visualizations and FFT analysis of fluctuating velocities have shown that an increase in TI does not affect the wake, vortex shedding frequencies and their patterns at low Reynolds numbers (134, 257 and 348). However, significant changes in wake widths were observed for $Re = 746, 933, 1244,$ and 1555 . The power spectra were also showed an increase in vortex shedding frequencies for $Re = 818, 3047$ and 4734 .

A change in wake patterns behind the circular cylinder was noticed with the change in cylinder diameters though the Reynolds numbers were kept constant. The shedding frequency was observed to be decreasing with an increase in diameter of the cylinder and reduction in free stream velocity. Further, the power spectra obtained at $Re = 4432$ with 25 mm diameter cylinder and at $Re = 4734$ with 7 mm diameter cylinder has shown that the effect of FST decreases with increase in diameter of the cylinder. This suggested that the diameter of the cylinder (that is, boundary layer thickness and its growth over the surface) plays a prevailing role in flow separation and wake transition for a given free-stream dominant frequencies. Hence, the certain range of FST frequencies and their amplitude can only influence the cylinder (delay separation) up to a certain diameter after which these disturbances are dissipated inside the boundary layer due to strong viscous action. It is essential to change the FST level and their amplitude to delay separation if the diameter of the cylinder is changed though the Reynolds number is kept constant. The effect of higher level of FST will be studied in future with an active grid arrangement.

Acknowledgements The authors acknowledge the Department of Science and Technology (DST), India for providing a partial financial support through FAST Track Young Scientist Scheme for carrying out the present work.

References

1. Y. Billah, R.H. Scanlan, Resonance, Tacoma narrows bridge failure, and undergraduate physics textbooks. *Am. J. Phys.* **59**(2), 118–124 (1991)
2. F.M. White, *Fluid Mechanics, McGraw-Hill Series in Mechanical Engineering*, 4th edn. (McGraw-Hill, New York, 1998), p. 296
3. B.R. Munson, F. Young, T.H. Okiishi, *Fundamentals of Fluid Mechanics*, 5th edn. (Wiley, New York, 2002), p. 526
4. C.H.K. Williamson, Vortex dynamics in the cylinder wake. *Annu. Rev. Fluid Mech.* **28**, 477–539 (1996)
5. H.J. Niemann, N. Hölscher, A review of recent experiments on the flow past circular cylinders. *J. Wind Eng. Ind. Aerodyn.* **33**, 197–209 (1990)
6. C.H.K. Williamson, R. Govardhan, Vortex-induced vibrations. *Annu. Rev. Fluid Mech.* **36**, 413–455 (2004)
7. J.A. Dutton, A.P. Hans, Clear air turbulence: a mystery may be unfolding. *Science* **167**, 937–944 (1970)
8. T.J. Mueller, L.J. Pohlen, P.E. Cnigliaro, B.J. Jansen Jr., The influence of free-stream disturbances on low Reynolds number airfoil experiments. *Exp. Fluids* **1**, 3–14 (1983)
9. P.W. Bearman, T. Morel, Effect of free stream turbulence on the flow around bluff bodies. *Prog. Aerosp. Sci.* **20**, 97–123 (1983)
10. W.Z. Sadeh, H.J. Brauer, A visual investigation of turbulence in stagnation flow about a circular cylinder. *J. Fluid Mech.* **99**, 53–64 (1980)
11. S.P. Suter, P.F. Maeder, J. Kestin, On the sensitivity of heat transfer in the stagnation-point boundary layer to free stream vorticity. *J. Fluid Mech.* **16**, 497–520 (1963)
12. K.C.S. Kwok, Turbulence effect on flow around circular cylinder. *J. Eng. Mech.* **112**(11), 1181–1197 (1986)
13. T. Murugan, M. Singh, V. Kumar, P.K. Chatterjee, Effect of free stream turbulence on sub-critical flow past a circular cylinder: an experimental investigation, in FMFP2015-5th International and 41st National Conference on Fluid Mechanics and Fluid Power, Paper no. 450, 12–14 Dec 2015
14. T.K. Sengupta, D. Das, P. Mohanamurally, V.K. Suman, A. Biswas, Modeling free-stream turbulence based on wind tunnel and flight data for instability studies. *Int. J. Emerg. Multi Discip. Fluid Sci.* **1**, 181–199 (2009)
15. T. Murugan, V. Kumar, D.L. Thanki, P.K. Chatterjee, A study on the decay of grid turbulence and its statistics using hot-wire anemometry, in FMFP2015-5th International and 41st National Conference on Fluid Mechanics and Fluid Power, Paper no. 452, 12–14 Dec 2015
16. H.S. Kang, S. Chester, C. Meneveau, Decaying turbulence in an active-grid-generated flow and comparisons with large-eddy simulation. *J. Fluid Mech.* **480**, 129–160 (2003)
17. L. Mydlarski, Z. Warhaft, On the onset of high-Reynolds-number grid-generated wind tunnel turbulence. *J. Fluid Mech.* **320**, 331–368 (1996)
18. W. Marzkirch, *Flow Visualization* (Academic Press, New York, 1977)
19. T. Asanuma, *Flow Visualization* (Hemisphere Publishing co., Tokyo, 1977)
20. D. H. Stedman, G. R. Carignan, *Flow visualization using ozone, Flow Visualization III* (Hemisphere, 1985)
21. M. Gharib, D. Kremers, M.M. Koochesfahani, M. Kemp, Leonardo's vision of flow visualization. *Exp. Fluids* **33**, 219–223 (2002)
22. B.M. Sumer, *Lecture Notes on Turbulence* (Technical University of Denmark, Denmark, 2005)
23. T. Murugan, A. K. Sonu, M. Singh, Subhendra, V. Kumar, R. P. Singh, P. K. Chatterjee, Measurement of turbulence statistics using hot-wire anemometry, in ICRTET 2014, International Conference on Recent Trends in Engineering and Technology, Cochin, India, 18–19 Jan 2014
24. H. Eckelman, The structure of the viscous sub-layer and the adjacent wall region in a turbulent channel flow. *J. Fluid Mech.* **65**, 439 (1974)
25. H. Tennekes, J.L. Lumley, *A First Course in Turbulence* (MIT Press, Cambridge, 1972)
26. U. Frisch, *Turbulence, the Legacy of A. N. Kolmogorov* (Cambridge University Press, Cambridge, 1995)
27. H. Schlichting, *Boundary Layer Theory*, 7th edn. (McGraw-hill, New York, 1979)
28. L.D. Landau, E.M. Lifshitz, *Fluid Mechanics*, 2nd edn. (Butterworth & Heinemann, Oxford, 1989)
29. F. Homann, Einfluss grosser zähigkeit bei stromung um zylinder. *Forschung auf dem Gebiete des Ingenieurwesens* **7**(1), 1–10 (1936)
30. L.S.G. Kovaszny, Hot-wire investigation of the wake behind cylinders at low Reynolds numbers. *Proc. R. Soc. Lond. A* **198**, 174–190 (1949)